International Journal of Cast Metals Research

ISSN: 1364-0461 (Print) 1743-1336 (Online) Journal homepage: https://www.tandfonline.com/loi/ycmr20

Heat transfer at the casting/chill interface during solidification of commercially pure Zn and Zn base alloy (ZA8)

G Ramesh & K N Prabhu

To cite this article: G Ramesh & K N Prabhu (2012) Heat transfer at the casting/chill interface during solidification of commercially pure Zn and Zn base alloy (ZA8), International Journal of Cast Metals Research, 25:3, 160-164, DOI: 10.1179/1743133611Y.0000000026

To link to this article: https://doi.org/10.1179/1743133611Y.0000000026

Published online: 12 Nov 2013.

Heat transfer at the casting/chill interface during solidification of commercially pure Zn and Zn base alloy (ZA8)

G. Ramesh and K. N. Prabhu*

Casting/chill interfacial heat transfer during solidification of commercially pure zinc and ZA8 alloy against copper, hot die steel, stainless steel and aluminium instrumented chills was investigated. The peak heat flux strongly depends on the thermophysical properties of chill, chill surface condition and superheat of the casting material. Contact angles of alumina coating measured on various substrates suggested that the adhesion of the coating material on copper chill was significantly better as compared to other chill materials. The heat flux curve in the case of coated chills is characterised by a double peak indicating remelting of the solidified casting shell. The second peak in the HTC curve is lower for high conductivity and higher for low conductivity chills as compared to the first peak. It is possible that solid shell formation and remelting occurred in the case of high thermal conductivity chills, whereas shell remelting did not happen in lower thermal conductivity chills.

Keywords: Casting/chill interface, Chill coating, Contact angle, Heat flux, Heat transfer coefficient

Introduction

Application of simulation technologies makes it possible to reduce design costs and ensure the quality of casting.[1] Casting solidification modelling requires heat transfer coefficients (HTCs) to identify the possible location of shrinkage defects. The success of simulating casting process is dependent on the accuracy of the metal/mould heat transfer data. The heat transfer at the casting/mould interface is not well understood. After the mould cavity is filled with the liquid metal, heat flow from metal to mould will result in a skin of solidified metal that is in contact with the mould. As solidification takes place, the thermal condition at the interface may change. The mechanism of heat transfer at a casting/mould interface is generally characterised by three stages:[2–5]

(i) perfect contact between the mould and the solidifying skin, and the heat transport is through conduction from liquid metal to the mould wall
(ii) imperfect contact between the mould and the solidifying skin, and the heat transfer is by conduction at the points of metal/mould contact, gaseous conduction and radiation across the microvoids
(iii) a gap of certain thickness separating the mould and solidifying skin may form at the later stages, resulting in a significant decrease in heat transfer.

A number of studies have been conducted to determine the interfacial HTCs between a solidifying casting and mould. These have shown that the values obtained can differ greatly depending on casting process variables like mould/chill material, casting material, superheat, casting configuration, mould/chill geometry, chill dressings, casting surface orientation and pressure.[6–13]

Bamberger *et al.* observed that a lower Si content in Al–Si alloys resulted in higher heat flux values and higher interface temperatures.[7] The same result has been obtained by Muojekwu *et al.*[6] They found that both heat flux and HTC increase with decreasing silicon content of the Al–Si alloy. The heat flux and HTC for Al–3Si and Al–5Si changed much more rapidly over the first 15 s as compared to Al–7Si alloy. Santos *et al.* reported that the initial values of interfacial HTC rise from about 1500 to 6000 W m^{-2} K^{-1} if the superheat is increased from 10 to 20% melting temperature for aluminium solidified against 60 mm thick steel chill.[8] Meneghini and Tomesani reported HTCs ranging from 4 to 8 kW m^{-2} K^{-1} for copper chills, 3–6 kW m^{-2} K^{-1} for aluminium chills and 1–2 kW m^{-2} K^{-1} for grey cast iron during sand casting of A356.[11] Studies by Prabhu *et al.* on mould dressings showed that the change in the coating material had a significant effect on mould thermal history.[12] The moulds coated with the graphite based mould wash exhibited a higher temperature compared with those coated with the alumina based mould coat. In addition, the graphite coated moulds showed higher heat flux transients compared with alumina coated moulds.

The experimental methods adopted by various researchers for the assessment of interface heat transfer were mostly based on the inverse heat conduction problem. Numerous investigations of metal mould interfacial heat transfer focused on aluminium and its alloys,[2–6,12,14] Sn–Pb alloys,[8–10] cast iron[15–17] and magnesium alloys.[18,19] There is very little literature concerning interfacial heat transfer during solidification of zinc base alloys. The present work is aimed at study of the effect of chill material, chill surface condition and superheat of casting on the casting/chill interfacial heat

Metallurgical and Materials Engineering, National Institute of Technology Karnataka, Surathkal, Mangalore, Karnataka 575025, India

*Corresponding author, email prabhukn_2002@yahoo.co.in

Received 22 May 2011; accepted 20 September 2011
DOI 10.1179/1743133611Y.0000000026

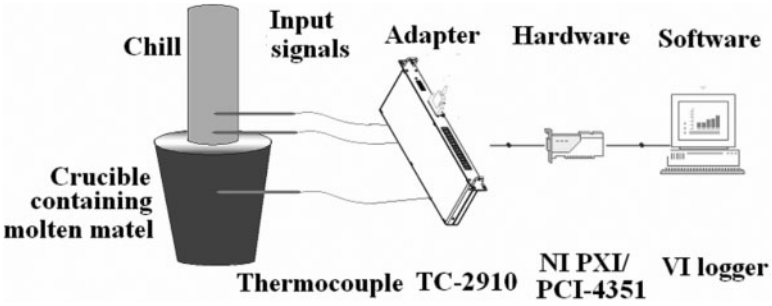

1 Schematic of experimental set-up of casting and chill during solidification

transfer during solidification of commercially pure zinc and ZA8 alloy.

Experimental

Commercially pure zinc and ZA8 alloy were used for solidification experiments. Copper, aluminium, hot die steel (H11) and stainless steel (304) were used as chill materials and instrumented with mineral insulated K type thermocouples. The dimensions of chill used are 100 mm in length and 25 mm in diameter. Two holes of 1 mm diameter were drilled on the interface of the chills at distances of 2 and 14 mm from the interface to accommodate thermocouples. The chill was heated to $\sim$150°C, and then alumina coating was sprayed onto its surface. The coating thickness was maintained at $\sim$800 μm. The thermophysical properties of the alloy and chill materials are given in Table 1, and the composition of the ZA8 alloy is given in Table 2.

In each experiment, $\sim$0·75 kg of alloy ingot is put in a preheated fireclay crucible and melted in an electric resistance furnace. Experiments were conducted at two different temperatures (460°C/510°C for ZA8 and 470°C/520°C for zinc) for all chill combinations. The alloy is maintained at these temperatures for $\sim$20 min to ensure complete melting. The crucible containing the molten alloy was quickly delivered to the insulated base of the solidification experimental set-up, and a twin bore ceramic beaded K type thermocouple was inserted into the melt. The instrumented chill was lowered into the crucible such that its bottom surface just comes in contact with the liquid melt. Temperature data from both casting and chill were recorded at 0·3 s interval using a computerised data acquisition system (NI PXI/ PCI-4351). A schematic sketch of the experimental set-up is shown in Fig. 1.

Table 1 Thermophysical properties of chill materials and casting alloys

Material	k/W m^{-1} K^{-1}	ρ/kg m^{-3}	c_p/J kg^{-1} K^{-1}
Chill			
Copper	385	8960	385
Aluminium	214	2698·9	900
Hot die steel	24·3	7800	460
Stainless steel	16·2	8000	500
Alloy			
ZA8	115	6300	435
Zinc	112	7100	390

Table 2 Chemical composition of ZA8 alloy

Al	Mg	Cu	Fe	Pb	Cd	Sn	Zn
8·2–8·8	0·02–0·03	0·9–1·3	0·035	0·005	0·005	0·002	Balance

Theoretical background

Heat flux transients are measured from the temperature history and thermophysical properties of the chill material by using the inverse method. The equation governing the two-dimensional transient heat conduction

$$\frac{\partial}{\partial x}\left(\lambda\frac{\partial T}{\partial x}\right)+\frac{\partial}{\partial y}\left(\lambda\frac{\partial T}{\partial y}\right)=\rho C_p\frac{\partial T}{\partial t} \quad (1)$$

was solved inversely using inverseSOLVER software. The macroscopic average HTC across the casting/chill interface h is calculated using equation

$$h=\frac{q}{(T_2-T_1)} \quad (2)$$

where q is the heat flux through the interface. T_1 and T_2 are surface temperatures of the chill and the casting respectively. The surface temperature of the chill was estimated by using inverseSOLVER.

Results and discussion

Thermal behaviour of chills

The thermal fields in the chill at different time steps is shown in Fig. 2. The gradual heating of the chill during the initial stage results in one-dimensional heat transfer within the chill, which then changes to two-dimensional temperature distribution. The heat transfer becomes one-dimensional in the final stage. It is observed that the heat flow changes from one- to two-dimensional at the time when the chill attains the peak temperature. The thermal field in stainless steel and copper chills shows one-dimensional heat transfer up to 1275 and 300 s respectively. The lower thermal conductivity and thermal diffusivity of stainless steel chill result in a slower conduction of heat from the casting/chill interface to top surface of the chill. The duration of two-dimensional heat transfer period for stainless steel chill is longer compared to copper chill due to its increased thermal resistance (L/k). The higher pouring temperature of the casting material results in the earlier occurrence of two-dimensional heat transfer in the chill. For example, the thermal field in copper chill indicates the start of two-dimensional heat transfer at 300 and 235 s for ZA8 casting poured at 460 and 510°C respectively. This is due to its increased rate of heating during solidification. The same behaviour is observed when casting zinc. The coating of chill offers extra resistance L_c/k_c and has a significant effect on heat flow, resulting in lower rate of heating of chill and delay the occurrence of two-dimensional heat transfer. It is observed that in coated

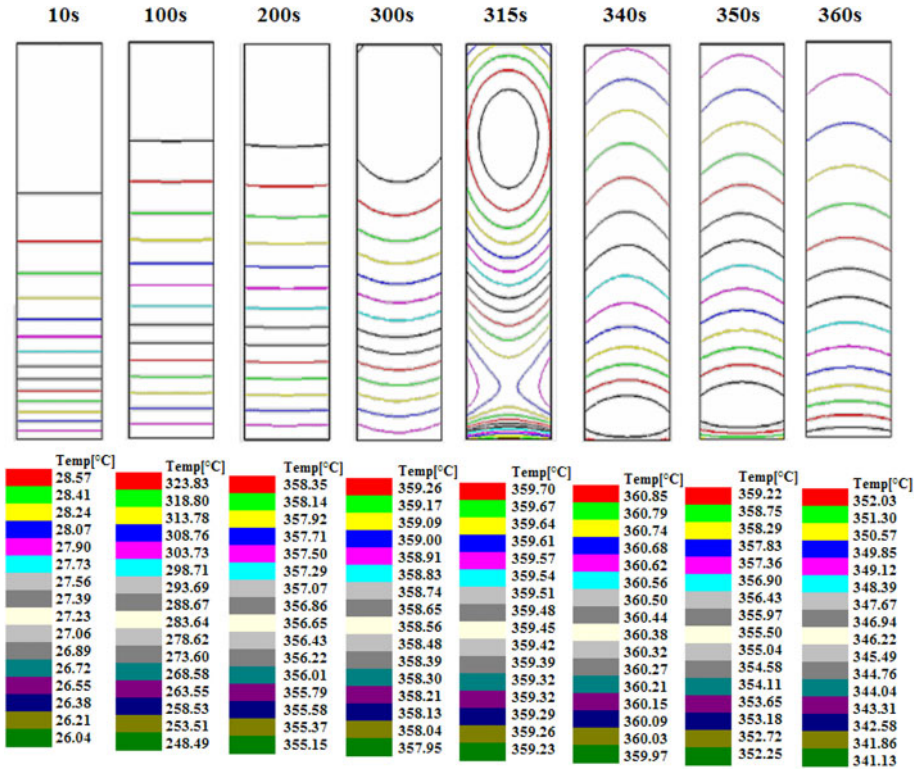

2 Thermal plots of copper chill at different time intervals during solidification of ZA8 casting (poured at 460°C)

chill, heat flow almost keeps one-dimensional during the entire solidification process.

Heat flux transients

For all the experiments, the heat flux shows a maximum shortly after pouring and then drops off rapidly (Fig. 3). Most of the previous works were carried out by researchers on aluminium alloys and showed the same trend. The initial heat flux value is high due to the good contact at the liquid metal/chill interface. As the casting started solidifying, the contact becomes non-conforming, resulting in a reduction in heat flux at the interface. The peak in the heat flux could therefore be associated with the beginning of solidification and was denoted by q_{max}. The time of occurrence of q_{max} marks the time of formation of a non-conforming contact at the casting/chill interface. It was found that for all types of casting/chill combinations, the peak heat flux increases with increasing pouring temperature. This was attributed to the improved interfacial contact between the melt and the mould surface and the increased initial driving force for heat transfer across the interface.[20] The casting material also had a significant effect on the peak heat flux. Zinc casting showed a higher heat flux than ZA8 casting. This is due to the higher heat capacity and melting temperature of zinc as compared to ZA8 alloy. The peak heat flux values of various casting/chill combinations are given in Table 3.

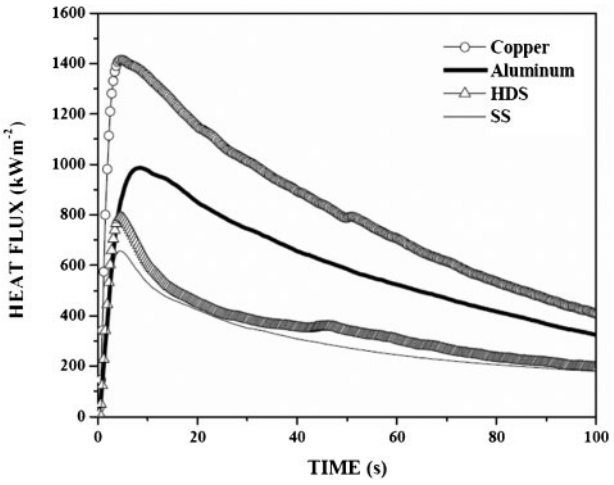

3 Heat flux versus time curve of ZA8 solidified against various chills: casting poured at 460°C

In coating experiments (Fig. 4), the heat flux transients showed a double peak during the solidification of casting. The initial contact between the coated chill and the casting results in the increase in heat flux. As solidification proceeds, the coating material gets heated and peels off from the chill surface, resulting in a non-conforming contact leading to rapid decrease in heat flux. After solidification, the casting surface showed the presence of coating material. The second peak may be attributed to the remelting of solidified solid shell. The differences between the first and second peaks and the time between two peaks are high in the case of coated copper chill and low in the case of coated stainless steel chill and intermediate for coated aluminium and die

Table 3 Estimated values of peak heat flux q_{max} for different chill materials

Peak heat flux/kW m^{-2}				
	ZA8 casting		Zinc casting	
Chill	460°C	510°C	470°C	520°C
Cu	1415	1810	1968	2062
Al	987	1237	1247	1329
HDS	790	835	763	1081
SS	657	758	702	948

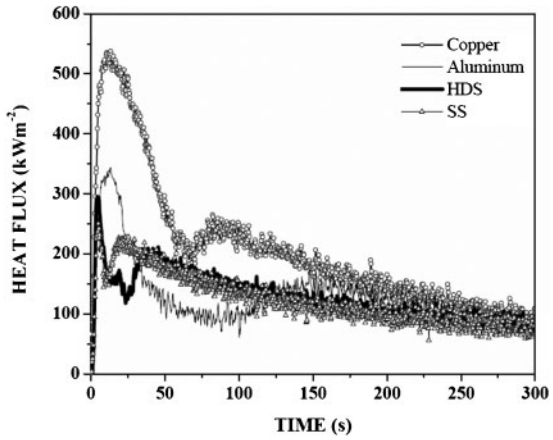

4 **Heat flux transients for ZA8 alloy solidified against alumina coated chill materials**

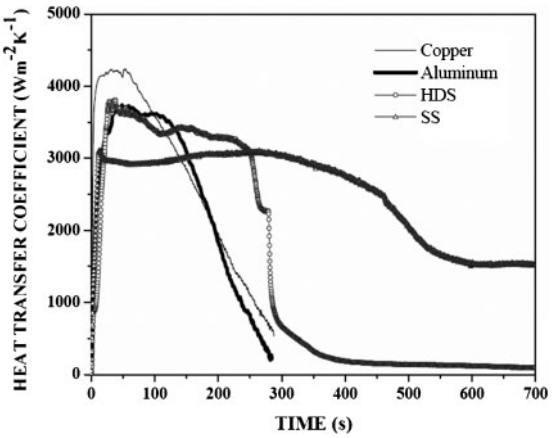

6 **Heat transfer coefficient versus time curve of ZA8 alloy solidified against various chills: casting poured at 460°C**

steel chills. For example, the difference between the first and second peaks and the time between two peaks are 272 kW m^{-2} and 69 s respectively for coated copper chill against ZA8 casting, whereas the corresponding values for coated stainless steel chill are 32 kW m^{-2} and 29 s. Contact angles of alumina coating measured on surfaces of various chill materials indicated that the wettability of the coating material on copper chill was significantly better as compared to other chill materials. The measured contact angle values of coating material droplets on copper, aluminium, hot die steel and stainless steel are found to be 25, 34, 41 and 54° respectively (Fig. 5). The adhesion characteristics of the coating material affected the peeling of the coating from the chill surface, and this influenced the time of occurrence of the second peak of heat flux transients. The coating on the chill material had a significant effect on the peak heat flux value. The presence of coating reduces the peak heat flux by ~37%.

Heat transfer coefficients

The variation of HTC with time is shown in Fig. 6. The peak HTCs were 4240, 3973, 3809 and 3104 W m^{-2} K^{-1} for ZA8 casting poured at 460°C and 6997, 6064, 5106 and 5009 W m^{-2} K^{-1} for zinc casting poured at 470°C solidified against copper, aluminium, hot die steel and stainless steel chills respectively. The peak HTC increases with increasing thermal diffusivity of the chill material. The increase in pouring temperature of the casting also increases the peak HTC values. For example, the peak HTCs were 6580, 5632, 5266 and 4281 W m^{-2} K^{-1} for copper, aluminium, hot die steel. and stainless steel chills respectively against ZA8 casting poured at 510°C.

The following stages are identified in the plot of variation of HTC with time (Fig. 7):

(i) stage I: in this stage, casting is completely liquid and has perfect contact with the chill surface. The casting surface temperature decreases sharply until it reaches the liquidus temperature. Correspondingly, the HTC rises gradually to a maximum value

(ii) stage II: when the casting reaches the liquidus, there is a change in slope of the curve due to liberation of latent heat. The formation of solid shell leads to non-conforming contact between the casting and the chill. The HTC was nearly constant during this period.

(iii) stage III: as the thickness of the solidified shell increases, its strength increases. This results in the contraction of the solidified shell from the chill, causing the formation of air gap. The HTC value in this stage continues to decrease.

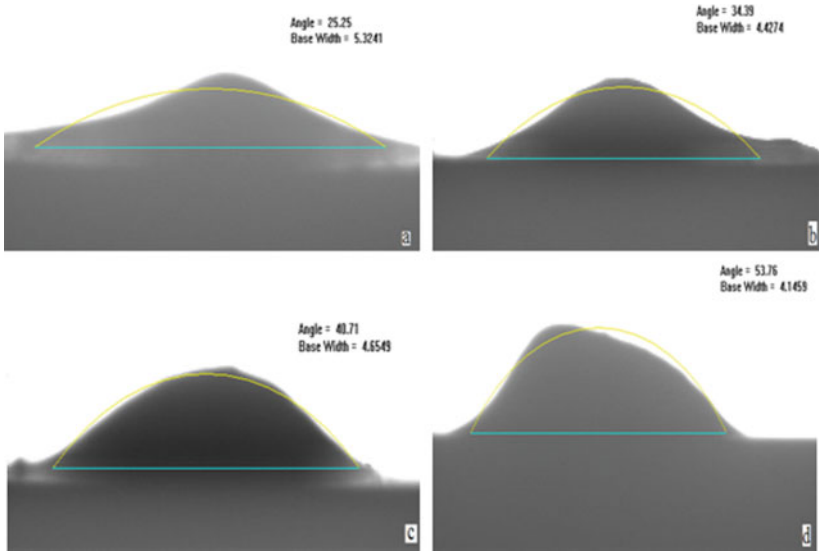

a copper; *b* aluminium; *c* hot die steel; *d* stainless steel

5 **Images of droplet of alumina coating solution spreading on different substrates**

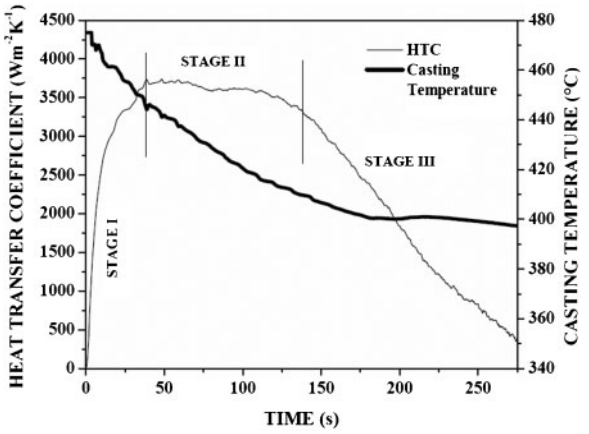

7 Variation of HTC and casting temperature versus time for ZA8 alloy solidified against aluminium chill

It is noted that the variation of HTC for the coated chill follows the same trend of heat flux due to the nearly one-dimensional heat flow. The chill coating reduces the peak HTC. It is observed that the value of the first peak in the HTC curve during solidification against high thermal conductivity coated chill was high compared to that of the second peak. The time of occurrence of the second peak is also higher (Fig. 8). An opposite trend is observed when casting is solidified against low thermal conductivity coated chills (Fig. 9). It is possible that solid shell forms and remelts in the case of a casting solidified against a higher thermal conductivity chill, whereas in the case of the casting solidified against a lower thermal conductivity chill, the remelting of solid shell is absent.

Conclusions

Based on the results and discussion, the following conclusions were drawn:

1. The thermal plot of chill indicated one-dimensional heat transfer within the chill during the initial stages of solidification that changes to two-dimensional when the chill attains peak temperature. It becomes one-dimensional again in the final stages. Heat flow was nearly one-dimensional in coated chills.
2. The heat flux transients showed a double peak during solidification of casting against coated chill. The second peak was attributed to the remelting of solidified solid shell.
3. The variation of HTC with time is characterised by three distinct regimes. The peak HTC increased with increasing thermal diffusivity of the chill material, pouring temperature of the casting and heat capacity of the casting material. The coating on the chill reduces the peak HTC.
4. Contact angles of alumina coating measured on surfaces of various chill materials indicated that the wettability of the coating material on copper chill was significantly better as compared to other chill materials.
5. A double peak in the HTC curve is observed during experiments involving coated chills. The solid shell formation and remelting occurs in the case of higher thermal conductivity coated chill, whereas in lower thermal conductivity chill, the remelting of the solid shell is absent.

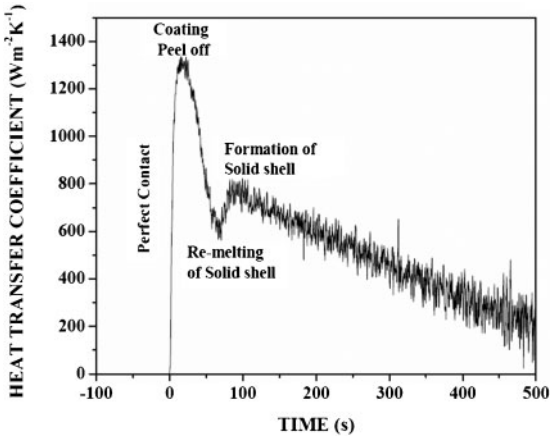

8 Variation of HTC with time for ZA8 alloy solidified against high thermal conductivity chill

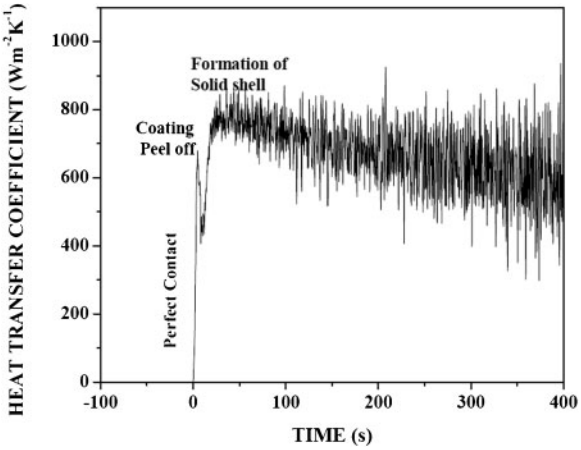

9 Variation of HTC with time for ZA8 alloy solidified against low thermal conductivity chill

Acknowledgements

The authors gratefully acknowledge the financial support provided by the Defense Research Development Organization (DRDO), Government of India, New Delhi, under an R&D project.

References

1. B. Cantor and K. O'Reilly: 'Solidification and casting'; 2003, Bristol, IOP Publishing Ltd.
2. K. Ho and R. D. Pehlke: *AFS Trans.*, 1984, **92**, 587–598.
3. K. Ho and R. D. Pehlke: *Metall. Mater. Trans. B*, 1985, **16B**, 585–594.
4. K. Ho and R. D. Pehlke: *AFS Trans.*, 1983, **91**, 689–698.
5. K. N. Prabhu and J. Campbell: *Int. J. Cast Met. Res.*, 1999, **12**, 137–143.
6. C. A. Muojekwu, I. V. Samarasekera and J. K. Brimacombe: *Metall. Mater. Trans. B*, 1995, **26B**, 361–382.
7. M. Bamberger, B. Z. Weiss and M. M. Stupel: *Mater. Sci. Technol.*, 1987, **3**, 49–56.
8. C. A. Santos, J. M. V. Quaresma and A. Garcia: *J. Alloys Compd*, 2000, **319**, 174–186.
9. I. L. Ferreira, J. E. Spinelli, B. Nestler and A. Garcia: *Mater. Chem. Phys.*, 2008, **11**, 444–454.
10. T. Chellaih, G. Kumar and K. N. Prabhu: *Mater. Des.*, 2007, **28**, 1006–1011.
11. A. Meneghini and L. Tomesani: *J. Mater. Process. Technol.*, 2005, **162–163**, 534–539.
12. K. N. Prabhu, B. Chowdary and N. Venkataraman: *JMEPEG*, 2005, **14**, 1–6.
13. J. C. Hwang, H. T. Chuang, S. H. Jong and W. S. Hwang: *AFS Trans.*, 1994, **102**, 877–884.
14. W. D. Griffiths: *Metall. Mater. Trans. B*, 1999, **30B**, 473–482.
15. K. N. Prabhu and W. D. Griffiths: *Int. J. Cast Met. Res.*, 2001, **14**, 147–155.
16. K. N. Prabhu and W. D. Griffiths: *Mater. Sci. Technol.*, 2002, **18**, 804–810.
17. F. Lau, W. B. Lee, S. M. Xiong and B. C. Liu: *J. Mater. Process. Technol.*, 1998, **79**, 25–29.
18. Z.-P. Guo, S.-M. Xiong, B.-C. Liu, M. Li and J. Allison: *Int. J. Heat Mass Transfer*, 2008, **51**, 6032–6038.
19. A. Hamasaiid, G. Dour, M. S. Dargusch, T. Loulou, C. Davidson and G. Savage: *Metall. Mater. Trans. A*, 2008, **39A**, 853–864.
20. K. N. Prabhu and K. M. Suresha: *JMEPEG*, 2004, **13**, 1–8.